



Comparing urban coastal flood risk in 136 cities under two alternative sea-level projections: RCP 8.5 and an expert opinion-based high-end scenario

Luis M. Abadie^a, Luke P. Jackson^b, Elisa Sainz de Murieta^{a,c,*}, Svetlana Jevrejeva^d, Ibon Galarraga^a

^a Basque Centre for Climate Change (BC3), 48940, Leioa, Basque Country, Spain

^b Climate Econometrics, Nuffield College Oxford University, Oxford, OX4 3QL, UK

^c Grantham Research Institute, London School of Economics and Political Science (LSE), London, WC2A 2AZ, UK

^d National Oceanography Centre, Liverpool, L3 5DA, UK

ARTICLE INFO

Keywords:

Regional sea-level rise
Coastal cities
Damage risk
Probabilistic projections
Ice-sheet melting risk
Unmitigated scenarios

ABSTRACT

The high degree of uncertainty associated with the extent of future sea-level rise stems primarily from the potential mass loss of the Greenland and Antarctica ice-sheets. We explore the impact of this uncertainty on economic damage due to sea-level rise for 136 major coastal cities. We compare the probability distribution for damage under the assumption of no adaptation for two relative sea-level projections: the RCP 8.5 scenario from the IPCC Fifth Assessment Report and a High-end scenario that incorporates expert opinion on additional ice-sheet melting. We use the 50th and 95th percentiles to estimate expected damage and one risk measure, the Expected Shortfall ES (95%), which represents the impact of low-probability, high-damage coastal flood risk (above the 95th percentile). Aggregate expected damage by 2050 under RCP 8.5 is US\$1,600 billion, while the aggregate risk measure ES(95%) is almost twice as much as the average damage at US\$3,082 billion. Under the High-end scenario, ES(95%) figures in Guangzhou and New Orleans by 2050 are twice as high as the expected damage. The city of Guangzhou leads the ranking under both scenarios, followed by Mumbai and New Orleans. Our results suggest that it is critical to incorporate the possibility of High-end scenarios into coastal adaptation planning for future sea-level rise, especially for risk-averse decision-making.

1. Introduction

Estimating the economic impact of future sea-level rise (SLR) provides important information for different stakeholders involved in coastal planning and climate change adaptation (Hinkel et al., 2015; Stammer et al., 2019). Producing such estimates is made more challenging by the uncertainty of SLR projections, yet they are highly relevant to policymakers in diverse regional contexts, who have different uncertainty tolerance and risk aversion levels (Hinkel et al., 2019). Information on the full range of uncertainty is thus useful in deciding when and how much adaptation is required (Haasnoot et al., 2019b) and what level of risk is acceptable or tolerable (Galarraga et al., 2018).

The economic impact of SLR and extreme events has been explored by many authors (e.g. Ciscar et al., 2011; Fu and Song, 2017; Hinkel et al., 2014; Scussolini et al., 2014). Hanson et al. (2011) estimate the

level of exposure to a 1-in-100-year extreme coastal event (storm surge) for 136 major coastal cities. They calculate that if global sea level rose 50 cm by 2070, the population exposed would triple and the asset exposure would increase by tenfold (in their study the term “flood” refers to the combination of SLR and storm surge). These calculations also consider population growth, urbanisation plans and, in some cases, subsidence. Hallegatte et al. (2013) calculate that average flood losses for the same 136 coastal cities could increase from US\$6 billion to US\$52 billion by 2050 due solely to socio-economic development (population and economic growth). In addition, they estimate that if subsidence occurred in delta cities coupled with a 20 cm global SLR and there was no adaptation of present-day defences, annual average losses could exceed US\$1 trillion by 2050. These losses would not be equally distributed: cities in South East Asia, on the East coast of Africa and on the East Coast of the USA would be hardest hit (Hallegatte et al., 2013;

* Corresponding author. Basque Centre for Climate Change (BC3), 48940, Leioa, Basque Country, Spain.

E-mail address: elisa.sainzdemurieta@bc3research.org (E. Sainz de Murieta).

<https://doi.org/10.1016/j.ocecoaman.2020.105249>

Received 22 September 2019; Received in revised form 20 April 2020; Accepted 1 May 2020

Available online 16 May 2020

0964-5691/© 2020 The Authors.

Published by Elsevier Ltd.

This is an open access article under the CC BY-NC-ND license

(<http://creativecommons.org/licenses/by-nc-nd/4.0/>).

Hanson et al., 2011).

The two studies mentioned have three main limitations: the first is the assumption that sea-level change is geographically uniform. Regional sea-level change can vary by as much as $\pm 30\%$ from the global average (Slangen et al., 2014), which means some coastlines experience higher than global average SLR (e.g. the US East Coast) while others experience lower than global average SLR (e.g. southern South America). Moreover, this variation is due solely to ocean volume and land-water/land-ice mass changes and to glacio-isostatic adjustment of the land surface, and does not consider local vertical land motion in the form of either natural (e.g. tectonic) or anthropogenic processes (e.g. groundwater extraction) that could increase or reduce the rate of relative sea-level change further (see Rovere et al., 2016). The second limitation lies in the calculation of annual average damage figures, which represent the expected damage in the most likely cases. Many authors have argued that focusing on expected damage may underestimate risk and may therefore not be suitable for guiding risk-averse decision making in coastal areas (Hinkel et al., 2015; Wong et al., 2017). The third caveat refers to how damage is calculated: at present this is done deterministically. This approach does not properly address uncertainty: the uncertainty of climate projections and socioeconomic impacts and their long time horizons requires, rather, the use of more sophisticated economic assessment tools that allow for uncertain risks, such as stochastic modelling, real option analysis or robust decision making (Markandya, 2014; Watkiss et al., 2015). Risk-based approaches as a basis for developing and informing public climate change adaptation policies have been adopted in London (which has defined a long-term plan to manage flood risk in the Thames Estuary over the course of this century (Ranger et al., 2013)) and more recently in New York City (Aerts et al., 2014; Horton et al., 2015).

The aim of our study is to estimate the economic risk of uncertain future SLR for the same set of 136 coastal mega-cities as studied previously by Hanson et al. (2011) and Hallegatte et al. (2013), but to overcome the limitations highlighted above.

To that end, we allow for regionally variable sea-levels by using two probabilistic relative sea-level projections derived from the same strong emissions scenario: Representative Concentration Pathway¹ (RCP) 8.5.² The first projection is the same as that calculated in IPCC AR5 (Church et al., 2013) and the second is a High-end projection that replaces the ice sheet components in Church et al. (2013) with those from an expert elicitation by Bamber and Aspinall (2013) (henceforth BA13, see Methods), taking into account the wide range in ice sheet projections (IPCC, 2019; Oppenheimer et al., 2019) and introducing as much as a 1 m difference in sea level projections at low probability by 2100 (Jackson and Jevrejeva, 2016). In other words, the High-end scenario accounts for the high-end of the uncertainty range in the contribution of ice-sheets to SLR, which distinguishes it from the IPCC AR5 RCP8.5 projection, particularly in the upper-tail, making it relevant when assessing future risk (Jevrejeva et al., 2014; Kopp et al., 2017). Different initiatives, management measures and investment projects in coastal areas require different types and levels of input data. Information about potential damage from upper-end sea-level changes may prove useful in assessing long-term investments and may be of use to those coastal managers with low risk and uncertainty tolerances, as suggested recently by Hinkel et al. (2019). Any other RCP data can of course also

be simulated with this method, but here the idea is to focus on risk adverse management, so we use the low probability, high impact emission scenario.

We utilise our updated stochastic modelling tools to estimate the full probability distribution of annual damage under uncertain sea-level rise projections. Abadie et al. (2017) and Abadie (2018) use an earlier version of these modelling tools to calculate risks of damage for 120 of the 136 coastal cities assessed here under three probabilistic relative SLR scenarios and show that low-probability, high sea-level projections point to potential losses up to 7 times greater than expected damage.

We estimate median (Expected) and 95th percentile (Value at Risk, VaR) annual damage for the sake of comparison with other published work, but we assess the risk of low-probability sea-level rises (Hull, 2018; Wilmott, 2014) using the Expected Shortfall (ES(95%)), which is the mean loss when the 95% percentile is exceeded. This risk measure is commonly used in financial economics to stress test systems and identify risk thresholds (Kupiec, 1998).

This study differs from Abadie et al. (2017) in four key ways: first, the focus here is on the difference between *expected damage* based on average values under most probable outcomes and *expected shortfall* estimates based on two SLR projections for the same emissions scenario (RCP 8.5) that encompass different perspectives regarding low-probability future ice-sheet changes. Second, the probabilistic damage model has been mathematically improved to give more accurate sea-level projections and projected losses for each city for the coming decades (see Methods). Third, we use different sea-level projections that consider a higher estimate of possible SLR than those of Kopp et al. (2014). Fourth, this study addresses impacts on 136 coastal mega-cities, compared to 120 in the previous paper.

2. Methodology

The following two subsections describe updates to our stochastic model that enable us to calculate different sea-level rise risk measures and how probabilistic SLR projections are calculated for the two scenarios in question.

2.1. The stochastic model of expected damage and risk calculation

Galarraaga et al. (2018) argue that risk-based approaches of this type could be used to stress test decisions on adaptation planning, in a similar way to tests carried out by the banking system (Blaschke et al., 2001). These methods have long been used in the banking sector to estimate the resilience of the whole system to different levels and types of financial risk. Similar approaches can be used for adaptation planning by analysing how a city's resilience may be affected by different risk situations. Considering high-end scenarios and taking a long-term perspective might prove to be relevant, given that economic, social and technical limits on adaptation are expected to increase with time (Haasnoot et al., 2019a).

In this study, we suggest using a Geometric Brownian Motion (GBM) model with variable coefficients over time to estimate SLR distributions in 136 coastal megacities. Financial risk methods in general, and Brownian motion theory in particular, can be useful in flood risk science (see Abadie et al., 2017; Hull, 2018 for further information). We select the GBM model (or diffusion process) because it allows sea-level figures to accelerate over time, i.e. the model can be applied in situations where the rate of SLR increases over time. This effect appears when the alpha (α) parameter in the GBM process is positive. The α parameter accelerates the increase in the expected value. Having a variable that is increasing over time is a common feature of IPCC SLR projections. This effect is clearly visible in worst-case scenarios such as RCP 8.5 (Church et al., 2013). This feature clearly indicates that this model is applicable.

The GBM model for SLR is calibrated using regional SLR data (50th and 95th percentiles for each city, time and scenario), to obtain the full probability distribution of damage as described below. The calculation

¹ According to the IPCC AR5, *Representative Concentration Pathways* (RCPs) are "scenarios that include time series of emissions and concentrations of the full suite of greenhouse gases and aerosols and chemically active gases, as well as land use/land cover". Note that the term "representative" means that "each RCP provides only one of many possible scenarios that would lead to the specific radiative forcing characteristics" (IPCC et al., 2014: 1771).

² RCP8.5 represents a "high (emission) pathway for which radiative forcing reaches greater than 8.5 W m^{-2} by 2100 and continues to rise for some amount of time" (IPCC et al., 2014: 1772).

process has the following steps:

- 1) First, 50th and 95th SLR percentiles are taken for 136 cities, 10 years and two scenarios (see [subsection 2.2](#)). The GBM generates a normal SLR distribution for each city, year and scenario. The parameters of the normal distribution (mean and volatility) can be easily calculated with the 50th and 95th percentiles using equations (2) and (3).
- 2) The next step is to use Monte Carlo simulations to calculate 2,720 probabilistic distributions of SLR resulting from modelling 2 scenarios, 136 cities and 10 decades. Simulating values for a normal distribution using the mean and the volatility is relatively straightforward. One million SLR values are calculated for each city, year and scenario with this technique.
- 3) Finally, earlier studies provide a cost function for each city that depends on time and SLR ([Hallegatte et al., 2013](#), henceforth called H13). Using the one million SLR simulations for each city, year and scenario from the previous step, it is possible to calculate one million cost values for each city, year and scenario. Using these millions of values, the mean of expected damage, the 95th percentile of damage and the average 5% worst cases (ES(95%)) can then be calculated.

2.1.1. Step 1: Calibration of the model using relative SLR percentiles

As explained above, we assume that sea level increases at any city and for every scenario follow a stochastic diffusion³ model of the Geometric Brownian Motion (GBM) type. The GBM with constant coefficients is a standard model in finance and is, in fact, the most commonly used stochastic process, as described in [Hull \(2018\)](#) and [Wilmott \(2014\)](#) (see Supplementary Information). Here, we use a modified GBM with variable coefficients. This version, as demonstrated in the supplementary material, enables us to ensure that for each time, city and scenario the process generates a normal distribution with the SLR percentiles used as inputs (50th and 95th).

Mathematically, this diffusion process is defined as presented in Equation (1):

$$dS_t = \alpha(t)S_t dt + \sigma(t)S_t dW_t \quad (1)$$

Where S_t is the SLR at time t ; $\alpha(t)$ is the drift parameter and $\sigma(t)$ is the volatility parameter, none of which is constant in this model; $dW_t = \varepsilon(t)\sqrt{dt}$ is the increment of a Wiener process with $\varepsilon(t) : N(0, 1)$.

Equation (1) has a deterministic part $\alpha(t)S_t dt$ and a stochastic part $\sigma(t)S_t dW_t$. The increase in $SLRdS_t$ at time t is due to the sum of these two components. The deterministic part in a short time dt causes an SLR proportional to $\alpha(t)$, S_t and dt . Note that at the next time, $t + 1$, this applies with a value S_{t+1} which, in a period no smaller than Δt , can grow exponentially (see Supplementary Material). The drift parameter $\alpha(t)$ informs about the expected SLR. The stochastic part enables values to be obtained that are different from those expected in simulations. The increasing or decreasing SLR caused by the stochastic part is, in a short time dt , proportional to $\sigma(t)$, S_t and $\varepsilon(t)\sqrt{dt}$. Note that obtaining random $N(0, 1)$ values for SLR means that this stochastic part can be simulated.

This model also differs from that in [Abadie et al. \(2017\)](#) in its use of different regionalised SLR data. In [Abadie et al. \(2017\)](#), SLR data are available for 2030, 2050 and 2100 and a continuous stochastic diffusion process with constant coefficients (alpha and sigma) is estimated. In that paper, the function cannot exactly meet both SLR percentiles (50th and 95th) at the three times using only two constant parameters. [Abadie et al. \(2017\)](#) present the best possible approximation that can be obtained with two constant parameters. Here, however, regionalised SLR data are estimated for every decade (see [subsection 2.2](#)). With the new

information per decade, a new model is needed in which the drift $\alpha(t)$ and volatility $\sigma(t)$ coefficients vary with time t . As a result, this new model exactly fits the 50th and 95th percentiles in every decade. This is a very substantial improvement on the earlier paper as it significantly enhances the precision of the estimates. That precision is improved by ensuring that exact SLR 50th and 95th percentiles are obtained at all times.

In order to calculate the log-normal distribution parameters at each time t , we consider the ten times that correspond to the decades of the 21st century. The model generates a log-normal distribution for each time t depending on the parameter functional forms $\alpha(t)$ and $\sigma(t)$. There are 136 cities, 2 SLR scenarios and 10 time moments, so we produce 2,720 different log-normal distributions of relative SLR. The model is calibrated using the median and the 95th percentile from the probabilistic SLR projections following equations (2) and (3). SLR projections are explained in [subsection 2.2](#) (see also Supplementary Information).

Next, two additional parameters are needed to model the log-normal distribution at each time t , measured at the end of each decade: the mean and the volatility. The *log-normal mean parameter* is the mean of the associated normal distribution and can be calculated using Equation (2):

$$\ln[\text{median}(S_t)] \quad (2)$$

The *log-normal volatility distribution parameter* at time t can be calculated using equation (3), where the 95th percentile divided by the median in the log-normal distribution is the error factor EF_t :

$$\frac{\ln EF_t}{1.645} \quad (3)$$

Note that in this model both parameters depend on time t .

2.1.2. Step 2: Monte Carlo simulation

Using the Monte Carlo technique it is now possible to simulate a normal distribution for each city, decade and scenario using the parameters calculated in Step 1. The procedure consists of obtaining random samples of the normal distributions with the parameters calculated in Step 1. In a few cases, the parameters of the log-normal distribution cannot be calculated directly using the median and the 95th percentiles because the log-normal distribution precludes negative values. These few cases include Athens and Helsinki and are found in the very first decades of the century. This issue is solved by changing the SLR scale for these cities. That is, the reference sea level is located so that the 5th percentile is zero; then after the Monte Carlo simulations, the value is restored by subtracting the original 5th percentile.

In the general case, we generate one million log-normally distributed random numbers using the mean and standard deviations previously calculated, which are extremely close to the input values used to generate the random numbers (see Supplementary Information). With this method, we thus obtain one million values of SLR for each city, scenario and decade.

2.1.3. Step 3: the damage function and the damage distribution

The damage distribution is based on two main components: the regionalised SLR resulting from the calibration process explained in Step 1 and the deterministic damage function as defined by H13.

The damage function developed by H13 includes three main components: (i) the effect of socio-economic development, which accounts for economic, urbanisation and population growth; (ii) a homogeneous global effect of subsidence in some cities only; and (iii) the effect of a certain amount of global mean SLR of 10 cm in 2030, 20 cm in 2050 and 30 cm in 2070. These values are applied equally to all cities, despite the different contexts and characteristics. For all these components, we replace the deterministic SLR proposed by H13 by the probabilistic relative SLR projections from [subsection 2.2](#), which are specific to each city (this process is illustrated in [Fig. S1](#)). In other words, we assume that the damage function has three components: one socio-economic, the second related to the local SLR projection and the third to subsidence in

³ A stochastic diffusion model represents a stochastic variable that evolves according to an equation describing its probabilistic behaviour over time ([Hull, 2018](#)).

each city. This is expressed in Equations 4 and 5.

$$D_t = f(S_t, t) \quad (4)$$

We assume that at time t the function is as follows:

$$D_t = f^1(t) + f^2(S_t) \quad (5)$$

Where $f^1(t)$ represents damage due to socio-economic growth and $f^2(S_t)$ represents the additional damage caused by sea-level rise and

2.2. Probabilistic sea-level rise projections

In the first-order one can sum individual sea-level components to give total, regional relative sea-level (RSL) change, which can be written as,

The contributions in Equation (1) can be placed in three groups: ocean volume changes due to globally averaged steric⁴ sea-level change

$$\begin{aligned} RSL(\theta, \phi, t) = & F_{SAL}(\theta, \phi) \cdot [STR(t) + DSL(\theta, \phi, t)] + F_{GLA}(\theta, \phi) RSL(\theta, \phi, t) = F_{SAL}(\theta, \phi) \cdot [STR(t) + DSL(\theta, \phi, t)] + F_{GLA}(\theta, \phi) \cdot GLA(t) + \\ & F_{GRE}(\theta, \phi) \cdot GRE(t) + F_{ANT}(\theta, \phi) \cdot ANT(t) + F_{LW}(\theta, \phi) \cdot LW(t) + F_{GIA}(\theta, \phi) \cdot t \cdot GLA(t) + F_{GRE}(\theta, \phi) \cdot GRE(t) + F_{ANT}(\theta, \phi) \cdot ANT(t) \\ & + F_{LW}(\theta, \phi) \cdot LW(t) + F_{GIA}(\theta, \phi) \cdot t. \end{aligned} \quad (6)$$

extreme events. As explained, the input data for this function is taken from H13 as a piecewise linear function for each time t . However, H13 assume a deterministic scenario of global mean sea-level rise, but here we incorporate the probability distribution of relative SLR for each city under RCP8.5 and the High-end scenario. An example of the damage function for the city of Abidjan is shown in Fig. 1, which shows how in this case damage particularly depends on the changes in sea level and, to a lesser extent, on time.

In this step we calculate a probability distribution of damage for each city that depends deterministically on socio-economic development $f^1(t)$ and stochastically on SLR and coastal extreme levels, $f^2(S_t)$. Note that the function does not include extreme events as a variable, but the initial expected damage obtained by H13 accounts for coastal extremes together with SLR. In other words, for a given city, the annual average damage obtained by H13 includes extreme events and SLR, which is known. To estimate the new probabilistic damage function we use the simulated values of normal distributions as calculated in Step 2 for each city, time and scenario instead of the fixed global SLR defined by H13. No adaptation is considered in the estimates.

The damage distribution is based on two main components: the regionalised SLR resulting from the simulation after the calibration process explained in Step 1 and the deterministic damage function as defined by H13. The damage distribution is built by combining the probabilistic local SLR projections under RCP8.5 and the high-end SLR scenario presented in subsection 2.2, with the deterministic damage function defined by H13. This gives probabilistic damage functions for 136 cities under the two aforementioned SLR scenarios for each decade until 2100. The probabilistic damage distribution enables expected damage to be calculated and the shape of the upper tail to be understood. The step-by-step process is explained below.

The simulated distribution with one million damage values obtained for each city and scenario and decade can be used to estimate the expected annual damage (i.e. the mean values of the distributions) and the Expected Shortfall (ES(95%)). The mean is an expected value but does not take into account that there is a 50% chance that the damage could be greater. The 95% percentile, also known as Value-at-Risk (VaR(95%)), shows with a 95% confidence level that the damage will not be exceeded in 95% of cases; in other words, VaR(95%) informs about where the worst cases start. However, VaR does not inform about the shape of the right tail. The Expected Shortfall (ES) is an alternative risk measure that mitigates some of VaR's flaws because it is the average of the 5% of worst cases and provides information about the shape of the right tail. It is a standard risk measure in financial economics that fits very well in this context (Abadie et al., 2017).

(STR), dynamic sea-level change (DSL) and the impact of self-attraction and loading (SAL) of the ocean upon itself due to long-term ocean density changes. Changes in ocean mass come from melting ice sheets (Greenland, GRE; Antarctic, ANT) and glaciers (GLA) and land-water storage/extraction (LW). Land-motion contributions come from Glacial Isostatic Adjustment (GIA), local tectonics and sediment compaction by anthropogenic/natural means. The latter two land-motion effects can significantly affect local sea-level projections but are not included in the global scale synthesis (see discussion). In Equation (1), each time-dependent (t), global average component (e.g. $ANT(t)$) is multiplied by its associated fingerprint (e.g. $F_{ANT}(\theta, \phi)$), which describes the gravitationally self-consistent ocean redistribution of water/ice-mass contributions (Mitrovica et al., 2001). θ and ϕ refer to latitude and longitude, while t refers to time relative to 1986–2005.

Jackson and Jevrejeva (2016) implement Equation (1) in a probabilistic framework for the two sea-level projections used in this study. The global average sea level components (e.g. $ANT(t)$) are each drawn from offline models, which have an associated probability distribution that varies over time (see Fig. 2 for distributions in 2100). Both RCP 8.5 scenarios use the global steric (Fig. 2a) and dynamic ocean components from the multi-model ensembles of RCP 8.5 in CMIP5 (Taylor et al., 2012), while glacier (Fig. 2b) and land-water (Fig. 2c) components are for RCP 8.5 from IPCC AR5 (Church et al., 2013) and GIA is from Peltier et al. (2015).

Although the IPCC AR5 (Church et al., 2013) and the Special Report on Oceans and Cryosphere in a Changing Climate (Oppenheimer et al., 2019) conclude that ice-sheets will continue to lose mass throughout the 21st century, the notion of uncertainty remains a prominent point of discussion for understanding both physical mechanisms and their response to changing climate. The uncertain range of ice sheet model projections is particularly important when trying to quantify low-probability future sea-level rise, especially for probabilistic projections. To fill this current knowledge gap, Bamber and Aspinall (2013) (henceforth BA13) use expert elicitation to provide judgements on ice-sheet processes, drivers and their trend throughout the 21st century. Their results give end-of-century probability distribution functions (PDFs) representing the sea level contribution of Greenland, East and West Antarctica which include a characterisation of the tails (<17th and >83rd percentiles; BA13). The median contributions are relatively consistent with IPCC central estimates but the upper tail (e.g. 95th percentile) is much higher (Fig. 2,e).

For the ice-sheet contributions of these two projections, we use the

⁴ Steric sea level changes: “sea level changes, both globally and locally, resulting from changes in water density (...). Density changes induced by temperature changes only are called *thermosteric*, while density changes induced by salinity changes are called *halosteric*” (IPCC et al., 2014: 1772).

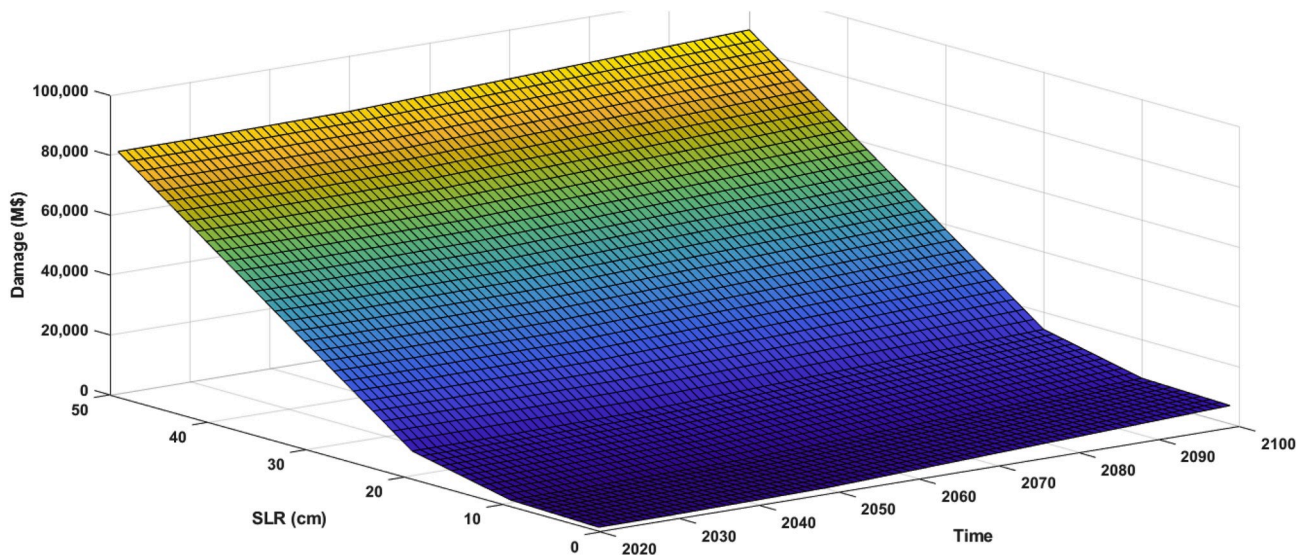


Fig. 1. Damage in the city of Abidjan as a function of sea-level rise and time.

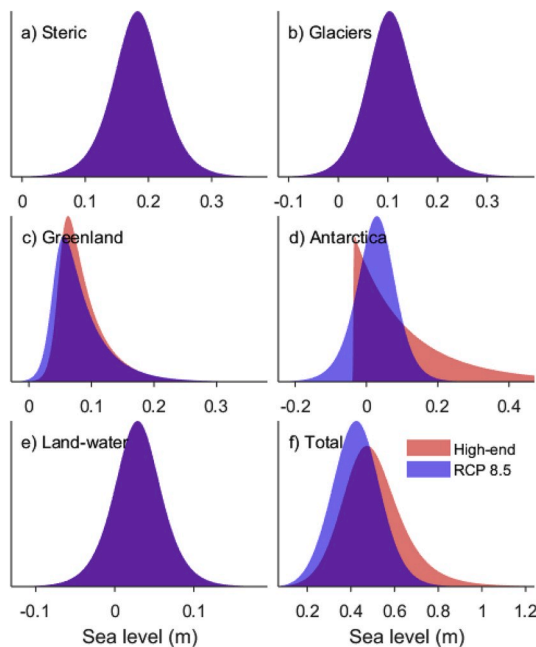


Fig. 2. Probability Densities of individual sea-level components projected contribution to global average sea level in 2070, a) Steric, b) Glaciers, c) Greenland, d) Antarctica, e) Land-water, and their sum (f) for RCP 8.5 (Church et al., 2013) and High-end scenarios (Jevrejeva et al., 2014). Purple indicates exact overlap of components. (For interpretation of the references to colour in this figure legend, the reader is referred to the Web version of this article.)

RCP 8.5 estimates from IPCC AR5 (Church et al., 2013) for the RCP 8.5 projection and the contributions from BA13 for the high-end projection (Fig. 2d and e). We sample each global sea-level component PDF and regionalise these values by their associated normalised sea-level fingerprints. We then sum across regionalised components (eq. (1)) for each sample and estimate quantiles for the ensemble of regional sea-level projections in each time slice. Each 1-degree grid point has a projected RSL time series from 2010 to 2100 in 10-year time slices, where each point in time has an associated probability distribution function (PDF).

3. Results

3.1. Expected damage

Our results show that relative sea-level projections in coastal areas for the two scenarios by 2070 differ by less than 20 cm at the median and ~80 cm at the 95th percentile (Fig. 3e and f). Differences between the two scenarios clearly emerge after the mid-century (Fig. S2). The spatial pattern of the regional sea-level projections is implicit in the range of city-based projections for 136 cities at the median (60 cm, Figs. S3) and 95th percentile (90 cm, Fig. S4).

Annual average (expected) damage estimates for the 15 most vulnerable cities for 2050, 2070 and 2100 are presented in Table 1 (ranked by expected damage by 2100 for RCP 8.5). The city with the highest expected damage is always Guangzhou (China), with an estimated figure of almost double those of the second and third-ranked cities (Mumbai and New Orleans). Expected damage in Guangzhou by 2050 could reach US\$331 billion under RCP8.5 and US\$420 billion under the high-end scenario, but by 2070 these figures are expected to double; by 2100, expected damage could reach US\$1.4 trillion under RCP 8.5 and US\$1.8 trillion the high-end scenario. The figures for expected damage for New Orleans and Mumbai by 2050 differ by US\$49 in one scenario and US\$50 billion in the other, though they could increase by a factor of 1.8 and 2.9 respectively by 2070 (a full list of cities and their expected damage estimates is shown in Supplementary Table S3).

3.2. Low probability risk: expected shortfall

The results for ES(95%) are presented in Fig. 2 (for 2070), Table 2 and Supplementary Tables S5–S8. As with expected damage, Guangzhou, Mumbai and New Orleans face the highest risks in both scenarios. However, the difference between RCP 8.5 and High-end sea-level projections by 2070 means a difference in risk of almost US\$ 900 billion for Guangzhou and more than US\$ 500 billion for Mumbai and New Orleans (Fig. 3f), with a fall to less than US\$ 325 billion for remaining cities. In addition to these three cities, by 2100 the High-end scenario shows an incremental risk of more than US\$ 500 billion for 16 cities compared to 9 cities for RCP 8.5. There is an increase of 16 cities from the RCP 8.5 scenario (70) to the High-end scenario (86) with Expected Shortfall exceeding US\$ 10 billion, which involves more than 60% of the cities analysed.

ES(95%) increases rapidly with time so under RCP8.5 the risk in Guangzhou exceeds US\$559 billion by 2050 and rises to more than US

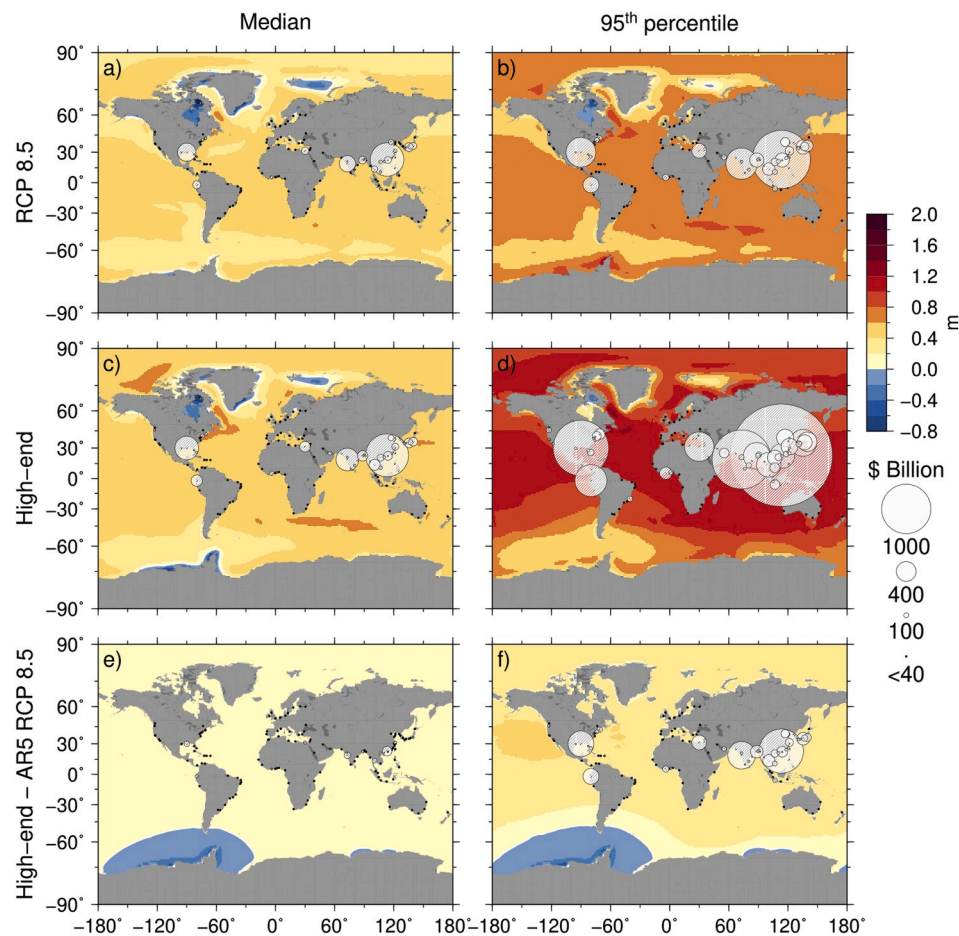


Fig. 3. Regional sea-level and city damages projected in 2070 for AR5 RCP 8.5 and High-end scenarios at median (a,c: expected damages) and 95th percentile (b,d: expected shortfall) and their differences (e,f).

Table 1

Ranking of cities according to their expected damages under the high-end and the RCP8.5 sea-level rise scenario. Damages are presented in billions of US dollars. Cities are ranked based on RCP8.5 in 2100.

Ranking	City	High-end scenario			RCP 8.5		
		2050	2070	2100	2050	2070	2100
1	Guangzhou Guangdong	419.9	869.9	1,782.2	330.8	678.1	1,392.3
2	Mumbai	162.2	459.8	976.4	112.4	328.5	734.5
3	New Orleans	258.1	478.9	907.5	209.2	369.1	673.7
4	Guayaquil	79.0	229.8	546.5	49.1	162.3	412.8
5	Alexandria	79.3	215.2	481.2	50.0	148.4	352.4
6	Shenzhen	68.1	197.9	460.0	42.0	141.5	346.4
7	Calcutta	90.7	211.6	452.2	65.9	156.8	346.4
8	Osaka-Kobe	120.9	224.9	431.3	101.1	180.9	342.3
9	Bangkok	62.0	177.7	415.8	38.7	125.3	312.5
10	Tokyo	96.2	178.0	341.7	79.8	141.7	270.4
11	Tianjin	60.4	138.7	283.8	45.5	104.4	219.5
12	Shanghai	32.4	115.7	287.3	15.7	78.0	212.1
13	Nagoya	76.4	135.4	258.0	64.1	109.2	204.1
14	Hai Phong	32.0	104.0	250.1	17.6	72.2	187.3
15	Abidjan	32.7	90.8	205.1	20.9	64.4	152.0

\$2.3 trillion by the end of the century. The trend in risk in Mumbai is similar, going from over US\$245 in 2050 to US\$1,3 trillion in 2100 (see [Tables S5–S8](#) for full data).

3.3. Per capita risk to cities

We calculate per capita expected damage in an effort to explore differences between cities. New Orleans, with a population that is

estimated to increase from 1.4 million in 2030 to 1.7 million in 2070, has projected expected damage per capita by 2030 ranging from US \$23,600 to US\$46,900 depending on the SLR scenario. These figures increase substantially by 2070 to between US\$218,000 and US \$283,000. The Chinese city of Guangzhou is second in the ranking, with expected per capita damage of US\$8,400–9,800 by 2030 and US \$42,600–54,600 by 2070. The third city in the ranking is Nagoya, in Japan, where damage increases tenfold from 2030 (US\$3,200–4,900) to

Table 2

Ranking of cities according to risk measured as Expected Shortfall, ES(95%), under the high-end and the RCP8.5 sea-level rise scenario. Damages are presented in billions of US dollars. Cities are ranked based on RCP8.5 in 2100.

Ranking	City	High-end scenario			RCP 8.5		
		2050	2070	2100	2050	2070	2100
1	Guangzhou Guangdong	902.9	2,077.1	4,731.5	559.8	1,179.0	2,392.3
2	Mumbai	451.3	1,197.1	2,794.0	245.2	636.5	1,354.9
3	New Orleans	513.0	1,126.6	2,558.0	307.3	602.5	1,089.7
4	Guayaquil	244.7	645.7	1,539.7	120.5	321.7	742.5
5	Alexandria	221.4	597.1	1,419.4	117.6	296.3	636.8
6	Shenzhen	207.0	547.8	1,315.6	107.3	286.0	635.9
7	Calcutta	217.1	540.0	1,247.0	131.2	288.1	614.1
8	Bangkok	189.4	503.6	1,208.3	98.7	251.6	577.4
9	Osaka-Kobe	231.6	499.2	1,108.7	153.1	289.7	558.3
10	Tokyo	183.5	393.1	861.1	123.9	233.2	439.4
11	Shanghai	122.9	351.2	862.6	55.7	174.7	404.4
12	Tianjin	137.7	338.2	767.7	82.2	184.7	382.2
13	Hai Phong	110.0	302.7	737.5	53.8	150.8	347.5
14	Nagoya	143.7	300.6	667.7	96.5	174.1	335.5
15	Abidjan	96.6	251.5	598.5	49.6	125.5	272.6

2070 (US\$34,400–42,600) (Table S10).

New Orleans leads the ranking of expected damage as a percentage of each city's GDP. By 2030 mean damage could reach 43–77% of GDP in New Orleans and by 2070 expected damage under the high-end scenario could reach 2.4 times its GDP. Six cities show expected damage estimates in excess of 10% of their GDP by 2030, but by 2070 the number rises to 17 and the top five cities in the ranking (New Orleans, Guangzhou, Nagoya, Hai Phong and Alexandria) could experience damage of more than 20% of their GDP under both SLR scenarios (see Table S11).

3.4. City characteristics impact damage more than sea-level variability

Expected damage and risk depend on the probability distribution of the sea-level rise scenario considered. It is interesting to recognise that there is nothing unusual about the cities highlighted through the text in terms of their projected future sea-level at the median (Fig. S3) or 95th percentile (Fig. S4); they lie well within the range of projections for other cities, which themselves are shown to experience future sea-level change that is greater than global average sea-level rise (Fig. 3). Despite the fact that SLR plays a greater role than socio-economic development in each city, as explained earlier, the spatial distribution of population and wealth for each city is also clearly a key factor, and one which is unique to each city. Note that this analysis is based on the estimates provided by H13, who used population data aggregated at 50 cm elevation levels to calculate the assets exposed via an estimate of the amount of capital per person. This capital per capita is obtained from the GDP per capita in each city and a ratio of “produced capital” to GDP, based on World Bank data (see H13).

To illustrate this point, the city projected to experience the highest future sea-level rise is New York (2.35 m at the 95th percentile under the High-end scenario). New York's expected damage by 2100 under AR5 RCP 8.5 is US\$111 and its expected shortfall is US\$181 billion. Though large, these figures are twelve times smaller than those of Guangzhou, where the expected damage and risk levels are US\$1.4 trillion and US\$2.4 trillion under RCP8.5 and US\$1.8 trillion and US\$4.7 trillion under the High-end scenario, where the low-probability, large increase in the Antarctic ice sheet contribution raises median RSL by 15 cm and 95th percentile RSL by 104 cm compared to AR5 RCP 8.5 (see Table S8).

3.5. The impact of land-motion

This analysis does not incorporate the effect of city-scale land-motion beyond that of GIA, which in most cases is small (<5 cm over the century). Uncertainty in the ice sheet component is most critical for many cities, but a small number face even greater short-term threats from

subsidence – much of which is anthropogenic in origin. Vertical land-motion varies over a range of spatial scales and can be natural (GIA, local tectonics, and sediment compaction) or anthropogenic (ground-water extraction, loading due to construction) in origin. At the suburban scale, streets or suburbs adjacent to each other can undergo land-motion with different signs (e.g. Dixon et al., 2006).

To assess the impact of localised land-motion on regional sea-level projections and damage, we correct our city-based projections by removing local land-motion due to GIA and replacing it with linearly extrapolated modern rates of subsidence from a database that we construct (see Supplementary Material for details). Subsidence not only amplifies the effect of future sea-level change but can completely dominate other components for cities with subsidence rates of centimetres to decimetres per year, such as Jakarta (3.3 m by 2040) and Ujung Padang (now known as Makassar, 3.7 m by 2040) (Fig. S8). The revised damage figures (Fig. S9) show a significant reordering of the top-ten most at-risk cities with Jakarta, New Orleans and Shanghai appearing 2nd, 3rd and 4th respectively. It is also apparent from this simple analysis that for many of these cities experiencing subsidence damage occurring by 2080 is now at the same level of risk likely to occur by around 2040 – a significant reduction of the planning horizon for tackling these issues.

A linear extrapolation of the estimated subsidence rates to the end of the century is perhaps a reasonable assumption for cities located on stable/incompressible substrates, but it should only be considered in the short term (next 10–20 years) for cities located on unstable/compressible substrates. For the latter (e.g. Jakarta) it is less accurate in the long term for a number of reasons: aquifer compaction causes steady land subsidence, but as the aquifer compaction limit is reached subsidence slows down (Chaussard et al., 2013). Furthermore, changes in anthropogenic behaviour that induce subsidence will alter subsidence rates (e.g., for Tokyo see Kaneko and Toyota, 2011). It is important to note that the spatial variability of vertical land motion means that the seafronts of cities can experience rates markedly different from those found inland, so inundation is less likely in these cases, in contrast to our simple approach.

4. Discussion

4.1. Comparing average expected damage to risk calculations (expected shortfall)

Compared to expected damage, risk (measured as Expected Shortfall ES(95%)), is systematically higher for the larger ice-sheet contribution after 2030 for the top-ten most vulnerable cities and for others. This fanning effect is most evident under the high-end scenario, where the

number of cities that could experience damage in excess of US\$450 billion by 2100 increases from 3 to 9 under RCP8.5 and from 7 to 18 under the high-end scenario (Tables S3 and S8). Aggregate expected damage under RCP 8.5 by 2050 is US\$1.6 trillion, while the aggregate ES(95%) is almost double the average damage at US\$3.082 trillion.

Under the High-end scenario, risks measured as ES(95%) by 2050 in Guangzhou and New Orleans are twice as high as expected damage. In Mumbai, the third city in the ranking, the risk of damage is 2.8 times the expected damage. Comparing risks to each city's GDP reveals that New Orleans leads the ranking, followed by Guangzhou ES(95%), Nagoya, Hai Phong and Alexandria, whose position in the ranking varies depending on the year and SLR scenario considered. For 2070, the risk-GDP ratio in New Orleans is 3.1 under RCP8.5 and 5.7 under the high-end scenario. In other words, risk could entail 3.1 to 5.7 times the amount of New Orleans' GDP. For the other four cities in the top five this ratio ranges between 0.6 and 1.4, whilst for the rest of the cities it is below 0.8 (see Tables S3 and S5 to S9). For 2050 the ES(95%) figures under the high-end scenario are 75% higher than under RCP8.5.

Abadie et al. (2017), who use relative SLR projections from Kopp et al. (2014), report figures for annual average damage under RCP8.5 by 2050 that are generally higher than our results in Table 1 and closer to the results under the high-end scenario, mainly due to differences in sea-level percentiles (see Table S4). For example, they put expected damage in Guangzhou at almost 30% higher than our estimates at US \$456 billion compared to US\$330.8 billion under RCP8.5 and US\$419.8 billion under the high-end scenario. H13 generally obtain lower damage: they find that in Guangzhou a 20 cm increase in sea level by 2050 would result in damage of US\$254.7 billion. We obtain a mean SLR for Guangzhou of 24 cm and expected damage of US\$330.8 billion.

For New Orleans, our results are higher than those of H13, but our SLR estimates are also larger by 5 cm under RCP8.5 and 10 cm under the high-end scenario. The differences with the estimates reported by Abadie et al. (2017) are even greater, but this can also be explained by the fact that the SLR projections obtained by Kopp et al. (2014) are almost three times as high as the RCP8.5 projection obtained in this study. The substantial differences between the results here and those in Abadie et al. for New Orleans, Calcutta, Osaka-Kobe and Bangkok can be attributed to local subsidence unaccounted for in this part of the study. A further discussion of subsidence and revised damage estimates is presented in subsection 3.5.

Expected Shortfall is also calculated by Abadie et al. (2017) for these cities under three RCPs, including RCP8.5. Their figures for damage are higher than those in Table 2 here and closer to those of the high-end scenario. For example, for 2050 they report an ES(95%) for Guangzhou of US\$1.06 trillion under RCP8.5. For New Orleans they obtain US \$934 billion, compared to US\$307 billion under RCP8.5 and US\$513 billion under the high-end scenario. This is again related to subsidence not considered in this part of our study.

4.2. Uncertainty: ice-sheet contribution to sea-level rise and future sea-level projections

Sea-level projections are the sum of multiple projected components (see Equation (1)), each estimated from independent modelling and each with an associated uncertainty due to modelling, internal variability, climate sensitivity, unresolved physics, etc. For example, the steric and dynamic sea-level components are estimated from CMIP5 model outputs, which are affected by model drift (which is generally small) and internal variability (which varies widely by location and across models). This can lead to differences of several decades in local emergence of RCP forcing above the non-anthropogenic background (Jackson and Jevrejeva, 2016). In this analysis, we use the same steric and dynamic sea-level components for the RCP 8.5 and High-end scenarios, so the role of model uncertainty is consistent from one to the other. Likewise, the projected sea-level contribution from glaciers and land-water storage is the same, so any uncertainty in either factor is

consistent from the RCP8.5 to the High-end scenario.

The ice-sheet uncertainties illustrated by using these two scenarios (modelled physics plus conservative dynamic estimate versus expert elicitation to allow for known unknowns) shows that accurately estimating the upper tail of the sea-level rise distribution is highly problematic.

Substantial progress has been made in increasing our understanding of the physical mechanisms driving ice sheet change, but many uncertainties remain. This is discussed at length in IPCC AR5 (Church et al., 2013) and IPCC SROCC (2019). In short though, while surface mass balance, i.e. the net difference between snowfall and surface melting, is a well-understood process with numerical simulations in agreement with observations (Fettweis et al., 2013; Lenaerts et al., 2012, 2016; Vernon et al., 2013), ice sheet dynamic mechanisms (e.g. debutching of ice shelves accelerating ice stream flow, ice cliff instability accelerating grounding line retreat) are less well understood and challenging to the model due to the complexity of the problem and computational demands (e.g. DeConto and Pollard, 2016; Fürst et al., 2015; Golledge et al., 2019; Joughin et al., 2012; Moore et al., 2013). Alternative modelling approaches include statistical-physical (Levermann et al., 2014; Ritz et al., 2015), statistical-probabilistic (Little et al., 2013) and statistical-emulator (Edwards et al., 2019) simulations, which have yielded a wide range of 21st century mass-losses (Greenland: 5–33 cm, Antarctica: 11–79 cm, (Oppenheimer et al., 2019)). The deep uncertainty associated with the contribution of ice-sheet dynamics to future sea level remains a key issue in the scientific community and is reflected in the more recent elicitation by Bamber et al. (2019), where the total sea-level contribution from ice sheets shows a widening of the likely range (17–83rd percentile) compared to BA13.

We recognise that the two scenarios selected are part of a wider set of possibilities (Le Cozannet et al., 2017) and that the lower the probability of exceedance is, the more uncertain the associated risk (in this case VaR and ES) is. However, if the RCP8.5 scenario is considered as a low end and the high-end scenario as representative of the deep uncertainty underlying ice-sheet behaviour, an analysis of the differences between them at least provides the decision-making community with a sense of the potential for avoided losses. To that end, we show the ratio of differences in median RSL and 95th percentile RSL projections versus the ratio of differences in ED and ES in Fig. 4.

Values exceeding 1 on the x-axis show that the difference in projected median RSL exceeds the difference in projected 95th p.c. RSL. Likewise, values exceeding 1 on the y-axis show that the difference in projected ED exceeds the difference in projected ES. As values get closer

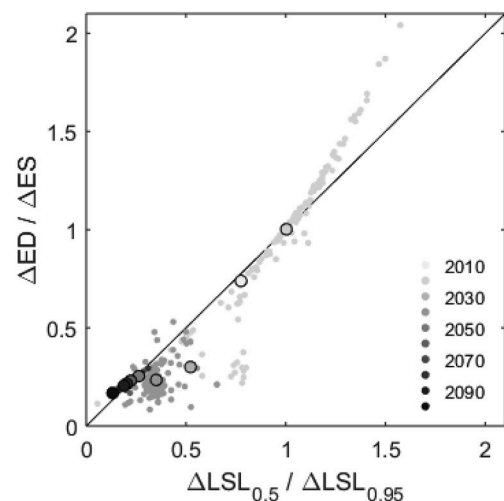


Fig. 4. Ratio of differences in median and 95th percentile relative sea level projections (LSL), versus the ratio of differences in expected damages (ED) and expected shortfall (ES).

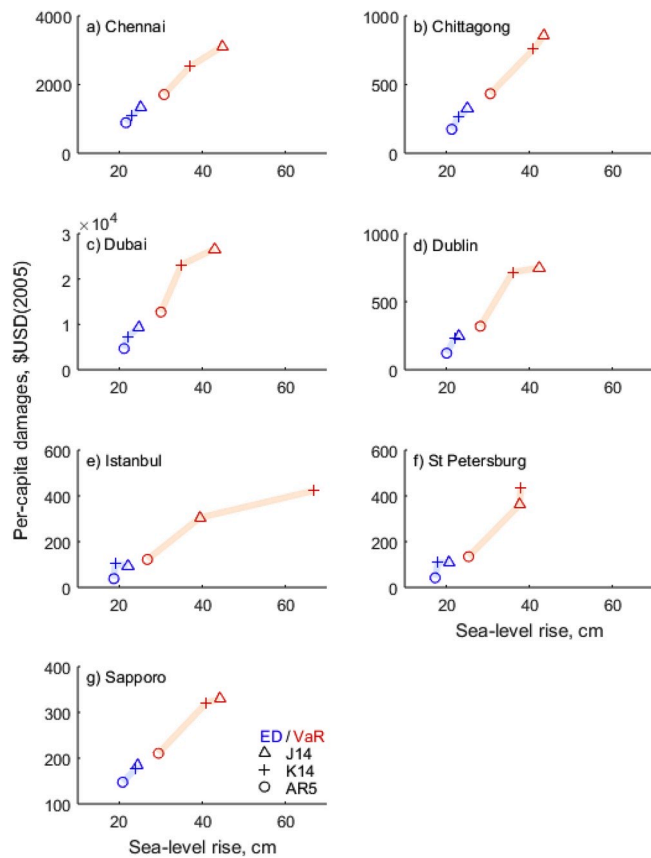


Fig. 5. Relative sea level versus per-capita damages for seven cities for IPCC AR5 RCP 8.5, Kopp et al. (2014) RCP 8.5 and High-end sea-level projections in 2050.

to 0 on the x- or y-axis, the difference in projected median RSL or ED becomes (much) smaller than projected 95th p.c. RSL or ES. More pertinently, while the difference between medians (RSL or ED) has a relatively narrow range over time (Fig. 5) it is really the increasing difference between 95th percentile in RSL projections (and by extension projected ES) that drives the ratios moving towards zero. The mean of these ratios across cities for each time slice is presented in the circles outlined, which show that the ratios (both axes) move towards zero and remain around 0.2 after 2050. Clearly, the scale of the differences between these two projected sea-level scenarios becomes substantial from the mid-century onwards, but these point cloud shapes indicate that the difference in damage is less sensitive to changes between projected sea-level as it falls below the 1:1 line around mid-century.

To further illustrate the sensitivity of the ice sheet component, we show RSL versus per-capita damage for seven cities for IPCC AR5 RCP 8.5, Kopp et al. (2014) RCP 8.5 and high-end sea-level projections for 2050 (Fig. 5). We are limited to using seven sites because Kopp et al. (2014) include land-motion in their projections. We therefore select sites with strong agreement for the median RSL projections for RCP8.5 (Kopp et al., 2014 use Church et al. (2013) for the median and likely range, and BA13 for tail behaviour). We have already shown in Fig. 2 that ice-sheet uncertainty is the major control propagating to sea-level uncertainty from the mid-century onwards, and this is confirmed in the ES with a much wider range, in some cases by a factor of three.

Uncertainty also arises in other parts of the methodology summed up in Equation (1), for example in the use of time-invariant land-ice/-water mass loss fingerprints. Jackson and Jevrejeva (2016) explore this issue by studying differences between projections with uniform land-ice mass loss and present-day land-ice mass loss patterns (which we use in this study). For most of the century, differences in all scenarios are less than

± 5 cm at both the median and 95th percentiles (Figs. S13–14 in Jackson and Jevrejeva, 2016). These differences are small, but their effect on damage may be significant depending on low-gradient exposure. Significant differences between sea-level projections only occur in the High-end scenario after 2060 for Southern South America (-45 cm), small islands in the Southern Ocean ($+50$ cm) and the United States, Southern Australia and Southern Africa (up to 15 cm) (Jackson and Jevrejeva, 2016).

Finally, we only select one present-day GIA field (ICE-6G_C (VM5a), Peltier et al., 2015) though there are multiple fields around the world that clearly show a range of solutions (Lambeck et al., 2003; Mitrović and Milne, 2003). Most GIA fields use a 1-dimensional viscoelastic structure which, though clearly not physically realistic, is acceptable as a first-order approximation. For the bulk of the world's oceans, the choice of GIA field has a negligible effect on projected sea-level change (Jackson and Jevrejeva, 2016). However, cities located in areas closer to former centres of deglaciation will have sea-level changes that differ by up to -5 cm and $+3$ cm from those presented here (e.g. Northern Canada, Scandinavia). As mentioned in the previous section, an incomplete picture of city-based land motion will inevitably affect the uncertainty associated with sea-level projections. A recent re-analysis of satellite elevation data (Kulp and Strauss, 2019) indicates that previous work underestimated global population exposure by a factor of three. Exploration of this update for city-level analysis is beyond the scope of this paper though it implies that our results and others published previously are likely to be a lower bound.

4.3. Uncertainty: socio-economic trajectories

Economic damage and risk measures are estimated based on a number of assumptions which add to the uncertainties related to SLR projections and the effect of subsidence. The economic growth data used in H13 were obtained using a general equilibrium model (OECD ENV-Linkages model) based on the assumption of “conditional convergence”, which implies that income levels in developing economies tend to converge with those of developed countries (H13, SM, p. 11). The general economic model considers 15 world regions and 22 economic sectors and is deterministic, so the data obtained represent a source of uncertainty.

Population growth is also a deterministic variable, and is assumed to increase proportionally across cities, but if coastal risk increases in a certain area it would be reasonable to think that either adaptation measures will be implemented or population and urbanisation processes in that area will be reduced. Nor is migration considered in these estimates, but coastal flooding has already been identified as a driver in certain countries such as China, India and Bangladesh (Neumann et al., 2015).

A new damage function in each city, with updated information and additional socio-economic variables, could provide a better picture of future coastal flood risk at city level. One particular area of development could be the application of alternative flood return period curves which might change damage projections for rare storm events whose uncertainty is comparable to or greater than those in sea-level projections for locations worldwide (Wahl et al., 2017). However, the database by H13 is very useful as it enables us to present and compare the scale of coastal flood risk across 136 megacities around the world. Although these sources of uncertainty exist, the method presented here allows for robust, in-depth analysis when updated or more detailed damage functions are developed.

5. Conclusions

This paper deals with the uncertainty related to the contribution of ice-sheets to SLR projections and shows that both the expected damage and the risk faced by cities worldwide increase dramatically. These results are very important for risk-averse coastal planners as they help

provide a far better understanding of the risk in each city and generate information needed to decide on the level of risk that each city is willing to accept. Finally, they give information on the scale of the uncertainties surrounding SLR projections. If long-term planning is needed, it seems essential to understand these uncertainties, which must be added to those related to socio-economic projections and subsidence for each city. When all sources of uncertainty are considered, the use of more robust analytical tools is justified.

We also show that stochastically modelling SLR enables us to better represent the damage and risk associated with SLR. Drawing on parallels in the banking system, we use the Expected Shortfall as an indicator of risk. This is well known in financial economics and can be extremely useful for appropriate risk management and risk governance. In particular, we propose that adaptation planning and other coastal planning decisions should undergo stress testing to provide a full understanding of the scale of the risk that planners are willing to accept. If sufficient adaptation is not foreseen, many cities in the world (especially in East Asia but also in the US) may have insufficient resources to recover from low-probability, high-impact extreme events. For instance, could New Orleans (US) recover from damage in 2070 equivalent to 3.1 times its GDP if a low-probability, high-impact coastal extreme event occurs? Or will Guangzhou be able to recover from an impact whose economic cost reaches US\$1.2 trillion by 2070? These questions remain to be answered but it is certainly very important to ask them.

Making good use of the information provided by this paper would certainly help to enhance the governance of the climate risks faced by cities.

Author attribution

L.M.A., L.P.J. and I.G.G. designed the research; L.M.A. and L.P.J. performed the modelling; L.M.A., L.P.J., E.S.M. and I.G.G. analysed the data; L.M.A., L.P.J., E.S.M. and I.G.G. and S.J. wrote the paper.

Declaration of competing interest

The authors declare that they have no conflict of interest.

Acknowledgements

L.M.A. is grateful for financial support from the Science and Innovation Ministry of Spain (MINECO RTI2018-093352-B-I00). L.P.J. acknowledges funding from the Robertson Foundation for Climate Econometrics (Grant Numbers: 9907422 and 9908921). E.S.M. acknowledges funding from the Basque Government (Postdoctoral Fellowship grant no. POS_2018_2_0027). I.G. was funded by the European Union's Horizon 2020 Research and Innovation Programme under grant agreement no. 776479 for the project CO-designing the Assessment of Climate CHange costs (COACCH.eu). L.M.A., E.S.M. and I.G. acknowledge support from the Basque Government through the BERC 2018–2021 programme and from the Spanish Ministry of the Economy and Competitiveness (MINECO) through BC3 María de Maeztu excellence accreditation (MDM-2017-0714). S.J. was funded by the Natural Environment Research Council under Grant Agreement No. NE/P01517/1.

Appendix A. Supplementary data

Supplementary data to this article can be found online at <https://doi.org/10.1016/j.ocecoaman.2020.105249>.

References

Abadie, L.M., 2018. Sea level damage risk with probabilistic weighting of IPCC scenarios: an application to major coastal cities. *J. Clean. Prod.* 175, 582–598. <https://doi.org/10.1016/j.jclepro.2017.11.069>.

- Abadie, L.M., Galarraaga, I., Sainz de Murieta, E., 2017. Understanding risks in the light of uncertainty: low-probability, high-impact coastal events in cities. *Environ. Res. Lett.* 12. <https://doi.org/10.1088/1748-9326/aa5254>.
- Aerts, J.C.J.H., Botzen, W.J.W., Emanuel, K., Lin, N., de Moel, H., Michel-Kerjan, E.O., 2014. Evaluating flood resilience strategies for coastal megacities. *Science* 344, 473–475. <https://doi.org/10.1126/science.1248222>.
- Bamber, J.L., Aspinall, W.P., 2013. An expert judgement assessment of future sea level rise from the ice sheets. *Nat. Clim. Change* 3, 424–427. <https://doi.org/10.1038/nclimate1778>.
- Bamber, J.L., Oppenheimer, M., Kopp, R.E., Aspinall, W.P., Cooke, R.M., 2019. Ice sheet contributions to future sea-level rise from structured expert judgment. *Proc. Natl. Acad. Sci. Unit. States Am.* 116, 11195–11200. <https://doi.org/10.1073/pnas.1817205116>.
- Blaschke, W., Jones, M.T., Majnoni, G., Martinez Peria, S., 2001. Stress Testing of Financial Systems: an Overview of Issues, Methodologies and FSAP Experiences (No. 01/08). International Monetary Fund.
- Chaussard, E., Amelung, F., Abidin, H., Hong, S.-H., 2013. Sinking cities in Indonesia: ALOS PALSAR detects rapid subsidence due to groundwater and gas extraction. *Rem. Sens. Environ.* 128, 150–161. <https://doi.org/10.1016/j.rse.2012.10.015>.
- Church, J.A., Clark, P.U., Cazenave, A., Gregory, J.M., Jevrejeva, S., Levermann, A., Merrifield, M.A., Milne, G.A., Nerem, R.S., Nunn, P.D., Payne, A.J., Pfeffer, T., Stammer, D., Unnikrishnan, A.S., 2013. Sea level change. In: Stocker, T.F., Qin, D., Plattner, G.K., Tignor, M., Allen, S.K., Boschung, J., Nauels, A., Xia, Y., Bex, V., Midgley, P.M. (Eds.), *Climate Change 2013: The Physical Science Basis. Contribution of Working Group I to the Fifth Assessment Report of the Intergovernmental Panel on Climate Change*. Cambridge University Press, Cambridge, pp. 1137–1216.
- Ciscar, J.-C., Iglesias, A., Feyen, L., Szabó, L., Regemorter, D.V., Amelung, B., Nicholls, R., Watkiss, P., Christensen, O.B., Dankers, R., Garrote, L., Goodess, C.M., Hunt, A., Moreno, A., Richards, J., Soria, A., 2011. Physical and economic consequences of climate change in Europe. *Proc. Natl. Acad. Sci. Unit. States Am.* 108, 2678–2683. <https://doi.org/10.1073/pnas.1011612108>.
- DeConto, R.M., Pollard, D., 2016. Contribution of Antarctica to past and future sea-level rise. *Nature* 531, 591–597. <https://doi.org/10.1038/nature17145>.
- Dixon, T.H., Amelung, F., Ferretti, A., Novali, F., Rocca, F., Dokka, R., Sella, G., Kim, S.-W., Wdowinski, S., Whitman, D., 2006. Subsidence and flooding in new Orleans: space geodesy. *Nature* 441, 587–588. <https://doi.org/10.1038/441587a>.
- Edwards, T.L., Brandon, M.A., Durand, G., Edwards, N.R., Golledge, N.R., Holden, P.B., Nias, I.J., Payne, A.J., Ritz, C., Wernecke, A., 2019. Revisiting Antarctic ice loss due to marine ice-cliff instability. *Nature* 566, 58–64. <https://doi.org/10.1038/s41586-019-0901-4>.
- Fettweis, X., Franco, B., Tedesco, M., van Angelen, J.H., Lenaerts, J.T.M., van den Broeke, M.R., Gallée, H., 2013. Estimating the Greenland ice sheet surface mass balance contribution to future sea level rise using the regional atmospheric climate model. *MAR. The Cryosphere* 7, 469–489. <https://doi.org/10.5194/tc-7-469-2013>.
- Fu, X., Song, J., 2017. Assessing the economic costs of sea level rise and benefits of coastal protection: a spatiotemporal approach. *Sustainability* 9, 1495. <https://doi.org/10.3390/su9081495>.
- Fürst, J.J., Goelzer, H., Huybrechts, P., 2015. Ice-dynamic projections of the Greenland ice sheet in response to atmospheric and oceanic warming. *Cryosphere* 9, 1039–1062. <https://doi.org/10.5194/tc-9-1039-2015>.
- Galarraaga, I., Sainz de Murieta, E., Markandya, A., Abadie, L.M., 2018. Addendum to 'Understanding risks in the light of uncertainty: low-probability, high-impact coastal events in cities. *Environ. Res. Lett.* 13, 029401. <https://doi.org/10.1088/1748-9326/aa513>.
- Golledge, N.R., Keller, E.D., Gomez, N., Naughten, K.A., Bernales, J., Trusel, L.D., Edwards, T.L., 2019. Global environmental consequences of twenty-first-century ice-sheet melt. *Nature* 566, 65–72. <https://doi.org/10.1038/s41586-019-0889-9>.
- Haasnoot, M., Brown, S., Scussolini, P., Jimenez, J.A., Vafeidis, A.T., Nicholls, R.J., 2019. Generic adaptation pathways for coastal archetypes under uncertain sea-level rise. *Environ. Res. Commun.* 1, 071006. <https://doi.org/10.1088/2515-7620/ab1871>.
- Haasnoot, M., Kwadijk, J., Alphen, J.V., Bars, D.L., van den Hurk, B., Diermanse, F., van der Spek, A., Essink, G.O., Delsman, J., Mens, M., 2019. Adaptation to uncertain sea-level rise; how uncertainty in Antarctic mass-loss impacts the coastal adaptation strategy of the Netherlands. *Environ. Res. Lett.* <https://doi.org/10.1088/1748-9326/ab666c>.
- Hallegatte, S., Green, C., Nicholls, R.J., Corfee-Morlot, J., 2013. Future flood losses in major coastal cities. *Nat. Clim. Change* 3, 802–806. <https://doi.org/10.1038/nclimate1979>.
- Hanson, S., Nicholls, R., Ranger, N., Hallegatte, S., Corfee-Morlot, J., Herweijer, C., Chateau, J., 2011. A global ranking of port cities with high exposure to climate extremes. *Climatic Change* 104, 89–111. <https://doi.org/10.1007/s10584-010-9977-4>.
- Hinkel, J., Church, J.A., Gregory, J.M., Lambert, E., Cozannet, G.L., Lowe, J., McInnes, K. L., Nicholls, R.J., Pol, T.D. van der, Wal, R. van de, 2019. Meeting user needs for sea level rise information: a decision analysis perspective. *Earth's Future* 7, 320–337. <https://doi.org/10.1029/2018EF001071>.
- Hinkel, J., Jaeger, C., Nicholls, R.J., Lowe, J., Renn, O., Peijun, S., 2015. Sea-level rise scenarios and coastal risk management. *Nat. Clim. Change* 5, 188–190. <https://doi.org/10.1038/nclimate2505>.
- Hinkel, J., Lincke, D., Vafeidis, A.T., Perrette, M., Nicholls, R.J., Tol, R.S.J., Marzeion, B., Fettweis, X., Ionescu, C., Levermann, A., 2014. Coastal flood damage and adaptation costs under 21st century sea-level rise. *Proc. Natl. Acad. Sci. Unit. States Am.* 111, 3292–3297.
- Horton, R., Little, C., Gornitz, V., Bader, D., Oppenheimer, M., 2015. New York city panel on climate change 2015 report chapter 2: sea Level rise and coastal storms: NPCC

- 2015 report chapter 2. Ann. N. Y. Acad. Sci. 1336, 36–44. <https://doi.org/10.1111/nyas.12593>.
- Hull, J., 2018. Options, Futures, and Other Derivatives, ninth ed. Global Edition. Pearson Education, Harlow.
- IPCC, 2019. IPCC Special Report on the Ocean and Cryosphere in a Changing Climate (in press).
- IPCC, 2014. Annex II: glossary. In: Barros, V.R., Field, C.B., Dokken, D.J., Mastrandrea, M.D., Mach, K.J., Bilir, T.E., Chatterjee, M., Ebi, K.L., Estrada, Y.O., Genova, R.C., Girma, B., Kissel, E.S., Levy, A.N., MacCracken, S., Mastrandrea, P.R., White, L.L. (Eds.), Climate Change 2014: Impacts, Adaptation, and Vulnerability. Part B: Regional Aspects. Contribution of Working Group II to the Fifth Assessment Report of the Intergovernmental Panel on Climate Change. Cambridge University Press, Cambridge, United Kingdom and New York, NY, USA, pp. 1757–1776.
- Jackson, L.P., Jevrejeva, S., 2016. A probabilistic approach to 21st century regional sea-level projections using RCP and High-end scenarios. Global Planet. Change 146, 179–189. <https://doi.org/10.1016/j.gloplacha.2016.10.006>.
- Jevrejeva, S., Grinsted, A., Moore, J.C., 2014. Upper limit for sea level projections by 2100. Environ. Res. Lett. 9, 104008. <https://doi.org/10.1088/1748-9326/9/10/104008>.
- Joughin, I., Alley, R.B., Holland, D.M., 2012. Ice-sheet response to oceanic forcing. Science 338, 1172–1176. <https://doi.org/10.1126/science.1226481>.
- Kaneko, S., Toyota, T., 2011. Long-term urbanization and land subsidence in asian megacities: an indicators system Approach. In: Groundwater and Subsurface Environments. Springer, Tokyo, pp. 249–270. https://doi.org/10.1007/978-4-431-53904-9_13.
- Kopp, R.E., DeConto, R.M., Bader, D.A., Hay, C.C., Horton, R.M., Kulp, S., Oppenheimer, M., Pollard, D., Strauss, B.H., 2017. Evolving understanding of antarctic ice-sheet physics and ambiguity in probabilistic sea-level projections. Earth's Future 5, 1217–1233. <https://doi.org/10.1002/2017EF000663>.
- Kopp, R.E., Horton, R.M., Little, C.M., Mitrovica, J.X., Oppenheimer, M., Rasmussen, D. J., Strauss, B.H., Tebaldi, C., 2014. Probabilistic 21st and 22nd century sea-level projections at a global network of tide-gauge sites. Earth's Future 2, 383–406. <https://doi.org/10.1002/2014EF000239>.
- Kulp, S.A., Strauss, B.H., 2019. New elevation data triple estimates of global vulnerability to sea-level rise and coastal flooding. Nat. Commun. 10, 1–12. <https://doi.org/10.1038/s41467-019-12808-z>.
- Kupiec, P.H., 1998. Stress testing in a value at risk framework. J. Deriv. 6, 7–24. <https://doi.org/10.3905/jod.1998.408008>.
- Lambeck, K., Purcell, A., Johnston, P., Nakada, M., Yokoyama, Y., 2003. Water-load definition in the glacio-hydro-isostatic sea-level equation. Quat. Sci. Rev. 22, 309–318. [https://doi.org/10.1016/S0277-3791\(02\)00142-7](https://doi.org/10.1016/S0277-3791(02)00142-7).
- Le Cozannet, G., Manceau, J.-C., Rohmer, J., 2017. Bounding probabilistic sea-level projections within the framework of the possibility theory. Environ. Res. Lett. 12, 014012. <https://doi.org/10.1088/1748-9326/aa5528>.
- Lenaerts, J.T.M., van den Broeke, M.R., van de Berg, W.J., van Meijgaard, E., Kuipers Munneke, P., 2012. A new, high-resolution surface mass balance map of Antarctica (1979–2010) based on regional atmospheric climate modeling: SMB Antarctica. Geophys. Res. Lett. 39. <https://doi.org/10.1029/2011GL050713>.
- Lenaerts, J.T.M., Vizzaino, M., Fyke, J., van Kampenhout, L., van den Broeke, M.R., 2016. Present-day and future Antarctic ice sheet climate and surface mass balance in the Community Earth System Model. Clim. Dynam. 47, 1367–1381. <https://doi.org/10.1007/s00382-015-2907-4>.
- Levermann, A., Winkelmann, R., Nowicki, S., Fastook, J.L., Frieler, K., Greve, R., Hellmer, H.H., Martin, M.A., Meinshausen, M., Mengel, M., Payne, A.J., Pollard, D., Sato, T., Timmermann, R., Wang, W.L., Bindshadler, R.A., 2014. Projecting Antarctic ice discharge using response functions from SeaRISE ice-sheet models. Earth System Dynamics 5, 271–293. <https://doi.org/10.5194/esd-5-271-2014>.
- Little, C.M., Oppenheimer, M., Urban, N.M., 2013. Upper bounds on twenty-first-century Antarctic ice loss assessed using a probabilistic framework. Nat. Clim. Change 3, 654–659. <https://doi.org/10.1038/nclimate1845>.
- Markandya, A., 2014. Incorporating climate change into adaptation programmes and project appraisal: strategies for uncertainty. In: Markandya, A., Galarraga, I., Sainz de Murieta, E. (Eds.), Routledge Handbook of the Economics of Climate Change Adaptation, Routledge International Handbooks. Routledge, New York, pp. 97–119.
- Mitrovica, J.X., Milne, G.A., 2003. On post-glacial sea level: I. General theory. Geophys. J. Int. 154, 253–267. <https://doi.org/10.1046/j.1365-246X.2003.01942.x>.
- Mitrovica, J.X., Tamisiea, M.E., Davis, J.L., Milne, G.A., 2001. Recent mass balance of polar ice sheets inferred from patterns of global sea-level change. Nature 409, 1026–1029. <https://doi.org/10.1038/35059054>.
- Moore, J.C., Grinsted, A., Zwinger, T., Jevrejeva, S., 2013. Semiempirical and process-based global sea level projections: GLOBAL SEA LEVEL PROJECTIONS. Rev. Geophys. 51, 484–522. <https://doi.org/10.1002/rog.20015>.
- Neumann, B., Vafeidis, A.T., Zimmermann, J., Nicholls, R.J., 2015. Future coastal population growth and exposure to sea-level rise and coastal flooding - a global assessment. PLoS One 10, e0118571. <https://doi.org/10.1371/journal.pone.0118571>.
- Oppenheimer, M., Glavovic, B.C., Hinkel, J., van de Wal, R., Magnan, A.K., Abd-Elgawad, A., Cai, R., Cifuentes-Jara, M., DeConto, R.M., Ghosh, T., Hay, J., Isla, F., Marzeion, B., Meyssignac, B., Sebesvari, Z., 2019. sea level rise and implications for low-lying islands, coasts and communities. In: Pörtner, H.O., Roberts, D.C., Masson-Delmotte, V., Zhai, P., Tignor, M., Mintenbeck, K., Nicolai, M., Okem, A., Petzold, J., Rama, B., Weyer, N. (Eds.), IPCC Special Report on the Ocean and Cryosphere in a Changing Climate (in press).
- Peltier, W.R., Argus, D.F., Drummond, R., 2015. Space geodesy constrains ice age terminal deglaciation: the global ICE-6G_C (VM5a) model: global Glacial Isostatic Adjustment. J. Geophys. Res.: Solid Earth 120, 450–487. <https://doi.org/10.1002/2014JB011176>.
- Ranger, N., Reeder, T., Lowe, J., 2013. Addressing ‘deep’ uncertainty over long-term climate in major infrastructure projects: four innovations of the Thames Estuary 2100 Project. EURO J Decis Process 1, 233–262. <https://doi.org/10.1007/s40070-013-0014-5>.
- Ritz, C., Edwards, T.L., Durand, G., Payne, A.J., Peyaud, V., Hindmarsh, R.C.A., 2015. Potential sea-level rise from Antarctic ice-sheet instability constrained by observations. Nature 528, 115–118. <https://doi.org/10.1038/nature16147>.
- Rovere, A., Raymo, M.E., Vacchi, M., Lorscheid, T., Stocchi, P., Gómez-Pujol, L., Harris, D.L., Casella, E., O’Leary, M.J., Hearty, P.J., 2016. The analysis of Last Interglacial (MIS 5e) relative sea-level indicators: reconstructing sea-level in a warmer world. Earth Sci. Rev. 159, 404–427. <https://doi.org/10.1016/j.earscirev.2016.06.006>.
- Scussolini, P., Tran, T.T.V., Koks, E., Diaz-Loaiza, A., Ho, P.L., Lasage, R., 2014. Adaptation to sea level rise: a multidisciplinary analysis for Ho chi minh city. Vietnam. Water Resour. Res. 53. <https://doi.org/10.1002/2017WR021344>.
- Slangen, A.B.A., Carson, M., Katsman, C.A., Wal, R.S.W. van de, Köhl, A., Vermeersen, L. L.A., Stammer, D., 2014. Projecting twenty-first century regional sea-level changes. Climatic Change 124, 317–332. <https://doi.org/10.1007/s10584-014-1080-9>.
- Stammer, D., van de Wal, R.S.W., Nicholls, R.J., Church, J.A., Le Cozannet, G., Lowe, J. A., Horton, B.P., White, K., Behar, D., Hinkel, J., 2019. Framework for high-end estimates of sea-level rise for stakeholder applications. Earth's Future 7 (8), 923–938. <https://doi.org/10.1029/2019EF001163>.
- Taylor, K.E., Stouffer, R.J., Meehl, G.A., 2012. An overview of CMIP5 and the experiment design. Bull. Am. Meteorol. Soc. 93, 485–498. <https://doi.org/10.1175/BAMS-D-11-00094.1>.
- Vernon, C.L., Bamber, J.L., Box, J.E., van den Broeke, M.R., Fettweis, X., Hanna, E., Huybrechts, P., 2013. Surface mass balance model intercomparison for the Greenland ice sheet. Cryosphere 7, 599–614. <https://doi.org/10.5194/tc-7-599-2013>.
- Wahl, T., Haigh, I.D., Nicholls, R.J., Arns, A., Dangendorf, S., Hinkel, J., Slangen, A.B.A., 2017. Understanding extreme sea levels for broad-scale coastal impact and adaptation analysis. Nat. Commun. 8, 16075. <https://doi.org/10.1038/ncomms16075>.
- Watkiss, P., Hunt, A., Blyth, W., Dyszynski, J., 2015. The use of new economic decision support tools for adaptation assessment: a review of methods and applications, towards guidance on applicability. Climatic Change 132, 401–416. <https://doi.org/10.1007/s10584-014-1250-9>.
- Wilmott, P., 2014. Paul Wilmott on Quantitative Finance. Wiley, Hoboken, N.J.
- Wong, T.E., Bakker, A.M.R., Keller, K., 2017. Impacts of Antarctic fast dynamics on sea-level projections and coastal flood defense. Climatic Change 144, 347–364. <https://doi.org/10.1007/s10584-017-2039-4>.